Pharm Res (2015) 32:47–60
DOI 10.1007/s11095-014-1443-y

RESEARCH PAPER

A Novel Strategy for Pharmaceutical Cocrystal Generation Without Knowledge of Stoichiometric Ratio: Myricetin Cocrystals and a Ternary Phase Diagram

Chao Hong • Yan Xie • Yashu Yao • Guowen Li • Xiurong Yuan • Hongyi Shen

Received: 16 March 2014 / Accepted: 10 June 2014 / Published online: 18 June 2014
© Springer Science+Business Media New York 2014

ABSTRACT

Purpose To develop a streamlined strategy for pharmaceutical cocrystal preparation without knowledge of the stoichiometric ratio by preparing and characterizing the cocrystals of myricetin (MYR) with four cocrystal coformers (CCF).

Methods An approach based on the phase solubility diagram (PSD) was used for MYR cocrystals preparation and the solid-state properties were characterized by differential scanning calorimetry (DSC), fourier transform-infrared spectroscopy (FT-IR), powder X-ray diffraction (PXRD), and scanning electron microscopy (SEM). The ternary phase diagram (TPD) was constructed by combining the PSD and nuclear magnetic resonance (NMR) data. After that, the TPD was verified by traditional methods. The dissolution of MYR in the four cocrystals and pure MYR within three different media were also evaluated.

Results A simple research method for MYR cocrystal preparation was obtained as follows: first, the PSD of MYR and CCF was constructed and analyzed; second, by transforming the curve in the PSD to a TPD, a region of pure cocrystals formation was exhibited, and then MYR cocrystals were prepared and identified by DSC, FT-IR, PXRD, and SEM; third, with the composition of the prepared cocrystal from NMR, the TPD of the MYR-CCF-Solvent system was constructed. The powder dissolution data showed that the solubility and dissolution rate of MYR was significantly enhanced by the cocrystals.

Conclusions A novel strategy for pharmaceutical cocrystals preparation without knowledge of the stoichiometric ratio based on the TPD was established and MYR cocrystals were successfully prepared. The present study provides a systematic approach for pharmaceutical cocrystal generation, which benefits the development and application of cocrystal technology in drug delivery.

KEY WORDS dissolution · myricetin · pharmaceutical cocrystals · preparation · ternary phase diagram

ABBREVIATIONS

API	Active pharmaceutical ingredient
CAF	Caffeine
CCF	Cocrystal coformer
CYA	4-Cyanopyridine
DSC	Differential scanning calorimetry
FT-IR	Fourier transform-infrared spectroscopy
HTS	High throughput screening
INM	Isonicotinamide
MYR	Myricetin
NIC	Nicotinamide
PSD	Phase solubility diagram
PXRD	Powder X-ray diffraction
SEM	Scanning electron microscopy

Electronic supplementary material The online version of this article (doi:10.1007/s11095-014-1443-y) contains supplementary material, which is available to authorized users.

C. Hong • Y. Xie (✉) • Y. Yao • X. Yuan • H. Shen
Research Center for Health and Nutrition, Shanghai University of Traditional Chinese Medicine, Shanghai 201203, China
e-mail: rosexie_1996@hotmail.com

G. Li
Pharmacy Department, Shanghai TCM-Integrated Hospital Shanghai 200082, China

Y. Yao
Institute of Chinese Materia Medica, Shanghai University of Traditional Chinese Medicine, Shanghai 201203, China

TPD Ternary phase diagram
USP United states pharmacopeia

INTRODUCTION

Utilization of noncovalent interactions for the development and designed self-assembly of individual molecules is an emerging frontier in research, and the formation of cocrystals has been previously explored in these fields. Pharmaceutical cocrystals are homogeneous solid phases containing an active pharmaceutical ingredient (API) and one or more neutral molecular components called a cocrystal coformer (CCF) in a crystal lattice with defined stoichiometry (1,2). Their design relies on the predictability of supramolecular interactions between the complementary functionalities of cocrystal components and results in heteromeric interactions over their homomeric counterparts (3). These heteromeric interactions are usually formed by hydrogen bonds, aromatic π-stacking, and van der Waals forces. Cocrystallization is a particularly attractive design strategy for solid API phases because it could modify some of the physicochemical properties of a candidate drug, such as solubility, dissolution rate, melting point, stability, and bioavailability (4). To date, at least 90 APIs have been targeted for pharmaceutical cocrystallization due to their undesirable solubility, stability, and inherent hydrogen bonding capability (5).

Myricetin (MYR), 3,3',4',5',5,7-hexahydroxyflavone (Fig. 1), is a flavonol that is present in many fruits, vegetables, and herbs, such as grapes, red wine, onions, berries, vine tea, and sargentodoxa cuneata (6–8). Recently, MYR was reported to exhibit potent iron chelating capacity, antioxidant and free-radical scavenging activities (9,10), as a result, it could be active against carcinogens in the body thus preventing mutations, and has potential for the treatment of diabetes, diarrhea, and thrombosis (11). However, the extremely low aqueous solubility (2 μg/mL) has limited its application in medicine. To improve an API's solubility or dissolution rate, salt formation or cocrystal formation is a common alternative approach, especially for acidic compounds like MYR, which contains 6 phenolic hydroxyl groups. Comparatively, MYR is not suitable for salt formation because MYR is a rather weak acid with a p*K*a of 6.63 and an unstable component in a basic environment (12), an appropriate salt former (a strong base) would aggravate MYR's instability. When salt formation is not optimal, cocrystallization is an alternative method for improving the physicochemical properties of an API because it features the formation of a complex between neutral molecules (13). Furthermore, MYR has many competitive hydrogen bonding sites, i.e., donors and acceptors (6 hydroxyls and 1 carbonyl), within its molecular framework, which provides the possibility for cocrystal formation of MYR with the proper CCFs. In this study, we opted for several pharmaceutically acceptable CCFs with relatively suitable structures to prepare pharmaceutical cocrystals of MYR to improve its poor solubility.

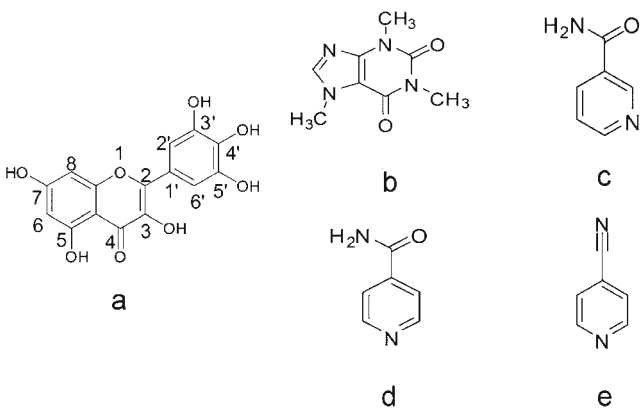

Fig. 1 Chemical structures of MYR (**a**) and CCFs: CAF (**b**), NIC (**c**), INM (**d**), CYA (**e**).

Previous approaches for screening and preparing cocrystals have advanced from being empirically based to a more efficient and rational basis. Currently, various preparation methods have been developed to obtain pharmaceutical cocrystals, and the solution and grinding methods are the most commonly used techniques (2). Generally, the types of CCFs and solvent have been considered during the process of cocrystal formation using these two methods; however, the stoichiometric ratio of the API and CCF, which is a critical factor, was usually fixed in many studies. For example, Dennis *et al.* (14) screened different CCFs and solvents to prepare the cocrystals of an API called compound 1 at two fixed stoichiometries (1:1 and 1:2) using high throughput screening (HTS) with a 96-well plate. Consequently, only two cocrystals with known stoichiometries were obtained: 1-benzoic acid cocrystal (1:1) and 1-maleic acid cocrystal (1:1). Although the majority of cocrystals have been reported to form at given ratios (1:1 and 1:2), other stoichiometries of individual components are also possible, such as acetazolamide-2,3-dihydroxybenzoic acid (3:1) (15), naproxen-nicotinamide (2:1) (16), cis,cis-1,3,5-cyclohexanetricarboxylic acid-urea (1:3) (17), and triphenylphosphine oxide-hydroquinone (2:3) (18). Accordingly, when fixing the stoichiometric ratio of an API and CCF during the screening and preparing process, other stoichiometric ratios are not tested. To obtain the cocrystals efficiently with all possible ratios, ratio selection should be carefully tested.

Ternary mixes, such as the API-CCF-Solvent system, can easily be presented using a ternary phase diagram (TPD) in which any point represents a fixed composition of the three substances. Such phase information can provide insight into the cocrystallization process, stability domains of various phases, and potential dissolution pathways (19). In addition, TPD could serve as a guide in selecting the proper solvent or

synthesis method for cocrystal formation and provide the basis for developing large-scale preparative procedures using solution crystallization (14). However, early methods for drawing the TPD involved allowing an API (CCF) and cocrystal to equilibrate in a solvent with varying CCF (API) ratios (20). Thus, the cocrystals are obtained before constructing its TPD in this method. These processes are tedious, and the native role of TPD could not be embodied such as directly guiding cocrystal preparation and scale-up when cocrystal is not quite available. Therefore, another problem that emerged in the study of cocrystals is how to construct the TPD before the cocrystals are successfully prepared, simultaneously apply the TPD for preparing pure powder cocrystals.

In this paper, the cocrystallization of MYR with four CCFs, caffeine (CAF), nicotinamide (NIC), isonicotinamide (INM), and 4-cyanopyridine (CYA) (Fig. 1), were investigated. Briefly, a streamlined strategy based on the principles of reaction cocrystallization (21) is discussed with the aim of preparing cocrystals without knowledge of the stoichiometric ratio and by simultaneously constructing their TPDs. Furthermore, the strategy was verified. The detailed physicochemical characterization, including differential scanning calorimetry (DSC), Fourier transform-infrared spectroscopy (FT-IR), powder X-ray diffraction (PXRD), scanning electron microscopy (SEM), and nuclear magnetic resonance (NMR), are also presented and discussed with an emphasis on the future development potential of the four cocrystals. Lastly, the dissolution of MYR in the four cocrystals and pure MYR was evaluated.

MATERIALS AND METHODS

Materials

The raw material (MYR) was purchased from Shanghai DND Pharm-Technology Co., Inc. (Shanghai, China). CAF, NIC, INM, and CYA were obtained from Sigma Aldrich Co. LLC (Shanghai, China). Methanol was purchased from Sinopharm Chemical Reagent Co., Ltd. (Shanghai, China). All chemicals were used as received without further purification.

Phase Solubility Diagram

The phase solubility of the MYR-CCF-solvent was determined by adding excess MYR to different concentrations of solutions of CCF while adding excess CCF to MYR. The resulting suspensions were allowed to reach equilibrium while stirring at 25°C. Aliquots of solutions were withdrawn after 12 h, centrifuged (13,000 rpm, 10 min), and the concentration of MYR and CCF in the supernatant were separately determined by HPLC (12).

Preparation of Cocrystals

In the pre-study, many candidate CCFs such as saccharin, caffeine, nicotinamide, isonicotinamide, 4-cyanopyridine, lysine, histidine, arginine, etc., were considered for MYR cocrystal preparation according to the cocrystal forming principle and cambridge structural database system. Eventually, only caffeine, nicotinamide, isonicotinamide, and 4-cyanopyridine could form pharmaceutical cocrystals with MYR. The detailed process for cocrystal preparation was as follows.

MYR-CAF. CAF (33.2 mg, 0.4% (w/w)) was dissolved in 10 mL of methanol (95.5% (w/w)). After, MYR (340.0 mg, 4.1% (w/w)) was added, and the mixture was stirred at 25°C for 12 h. The precipitate was obtained by suction filtration and dried in a fume hood for 24 h at room temperature. The other three cocrystals were prepared at the same temperature, feeding process, and post-processing except for the percentages of API, CCF, and solvent.

MYR-NIC. MYR (173.5 mg, 2.0% (w/w)), NIC (581.2 mg, 6.7% (w/w)), methanol (10 mL, 91.3% (w/w)).

MYR-INM. MYR (284.1 mg, 3.3% (w/w)), INM (404.6 mg, 4.7% (w/w)), methanol (10 mL, 92.0% (w/w)).

MYR-CYA. MYR (317.1 mg, 3.7% (w/w)), CYA (334.2 mg, 3.9% (w/w)), methanol (10 mL, 92.4% (w/w)).

Differential Scanning Calorimetry (DSC)

A differential scanning calorimeter (822e, DSC instruments, Mettler Toledo, Switzerland) was used to perform thermal analysis on the samples of MYR, CCFs, and MYR cocrystals. Powder samples of approximately 3.0 mg were placed in open aluminum crucibles and heated at a rate of 10°C/min up to 400°C.

Powder X-Ray Diffraction (PXRD)

The PXRD patterns of MYR, CCFs, and MYR cocrystals were obtained at ambient temperature using a Shimadzu XRD-6000X (Shimadzu, Japan). The samples were irradiated with Ni-filtered Cu-K (α) radiation at a voltage of 40.0 kV and a current of 40.0 mA. The scanning rate was 2°/min over a diffraction angle of 2θ ranging from 3° to 50°.

Fourier Transform-Infrared Spectroscopy (FT-IR)

FT-IR spectra were recorded on a Nicolet FT-IR-R330 spectrophotometer (ThermoFisher Scientific, Massachusetts, USA) over a range of 4,000 cm^{-1} to 450 cm^{-1} with a resolution of 1 cm^{-1} and 64 scans. MYR, CCFs, and MYR cocrystals were prepared in KBr disks with a hydrostatic press at a force of 5.2 T/cm^2 for 3 min.

Scanning Electron Microscopy (SEM)

Morphological evaluation was performed using SEM (Philips XL-30, Eindhoven, Holland). A small piece of double-sided adhesive tape was fixed onto an aluminum stub, and the MYR and MYR cocrystal powders were sprinkled and dispersed on the stub surface. Prior to examination, the samples were sputter coated with gold-palladium under argon atmosphere to render them electrically conductive.

Nuclear Magnetic Resonance (NMR) Spectroscopy

^{1}H-NMR spectra were acquired on a Bruker Avance III 600 MHz spectrometer equipped with a 5-mm PABBO probe (Bruker Corporation, Fällanden, Switzerland) at 25°C. Typically, approximately 10 mg of MYR, CCFs, and MYR cocrystals were dissolved in a glass vial in 0.5 mL of DMSO-d_6. After, the solution was transferred into an NMR tube. All data were acquired and processed using Bruker Topspin 3.0 software.

Transition Concentration (C_{tr}) Measurement (Verification)

The transition concentration or invariant point was validated using a previously reported method (22). This was achieved by adding excess cocrystals to a saturated MYR solution containing excess solid MYR or a saturated CCF solution with excess solid CCF. After equilibration for 12 h, the supernatants were withdrawn and quantified by HPLC as described in the "Phase Solubility Diagram" section, and the obtained solid phases were characterized using DSC or PXRD. The verification experiments for the two C_{tr} values were performed in triplicate.

Powder Dissolution Experiments

For the dissolution studies of MYR and MYR cocrystals in powder, all samples were sieved through a 178-μm screen to produce powders with a similar range in particle sizes. The tests were performed on an RCZ-6C1 (Huanghai Medicine & Drug Testing Instruments, Shanghai, China) using the United States Pharmacopeia (USP) paddle apparatus II. The rotational speed of the paddle was set at 100 rpm and a temperature of the dissolution media was maintained at 25 ± 0.5°C. Accurately weighed powders corresponding to 50 mg of MYR were added to dissolution vessels containing 300 mL of medium. Three dissolution media were studied: 0.1 mol/L HCl (pH 1.2), 0.1 mol/L acetate buffer (pH 4.5), and 0.05 mol/L phosphate buffer (pH 6.8). Sampling was performed at 10, 20, 40, 60, 120, and 240 min, and the withdrawn slurry was filtered using 0.45-μm cellulose filters. A 20-μL sample was injected into an HPLC to quantify the concentration of MYR as mentioned in the "Phase Solubility Diagram" section. All tests were performed in triplicate.

RESULTS AND DISCUSSION

Phase Solubility and Preparation of the Solid Phases

The phase solubility diagram (PSD) shows the concentrations of reactant in solution when different solid phases (API, cocrystal, and CCF) are at equilibrium, which was useful for determining the solution composition in specific phases and for studying solution complexation (23). Thus, we can ensure the formation of a new phase by observing the change in trends of the concentration curve in the PSD, which can also be used for directing the synthesis of cocrystals. The concentration of reactant in the PSD is the total concentration, which is originated from the unbound reactant and bound reactant, but it actually represents the saturation concentration at equilibrium. From this point, it is presumable that the cocrystal PSD could be constructed by adding an API and CCF to a proper solvent as long as the number of reaction ratios of the API and CCF was enough and that excess solid existed when the system was at equilibrium. Here, we used NIC as an example to explain our strategy for cocrystal preparation using the PSD. Considering the poor aqueous solubility of MYR and the preliminary experimental results (data not shown), methanol was selected as the solvent to prepare MYR cocrystals.

Figure 2 presents the PSD of the MYR-NIC-Methanol system, in which point a and b represent the solubility of MYR and NIC in neat methanol, respectively. From the obtained points in the PSD, the concentration of MYR decreased with the increase in NIC concentration when all phases reached equilibrium in methanol. The curve could be divided into three stages after all points were connected, in which the solid lines ac_1 and c_2b represent the solubility of MYR and NIC in different solutions, respectively. Furthermore, the trend of ac_1 and c_2b were relatively smoother compared to c_1c_2, which indicated that the solubility of MYR (ac_1) and NIC (c_2b) were less affected by the presence of the other component (NIC (ac_1) or MYR (c_2b)). However, as shown in line c_1c_2, the concentration of MYR (NIC) falls quickly when the concentration of NIC (MYR) is increased

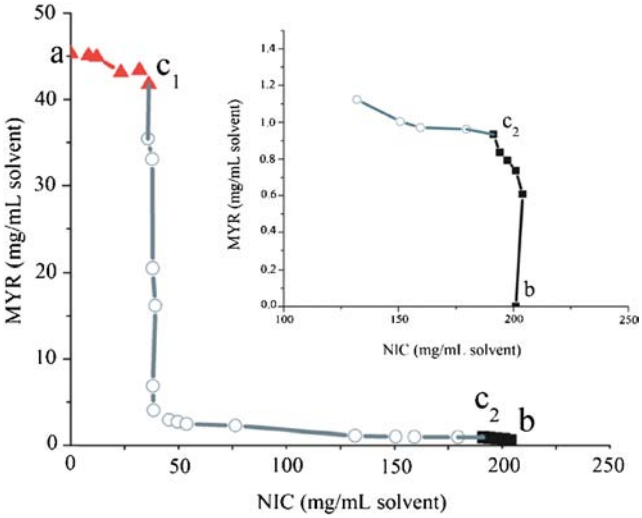

Fig. 2 PSD for the MYR-NIC-Methanol system at 25°C. The concentrations of reactant (MYR and NIC) in solution at equilibrium are shown in the PSD. "a" and "b" represent the solubility of MYR and NIC in methanol, respectively. "c_1" and "c_2" represent the transition concentration.

in the system, which indicated a new cocrystal might be formed, and c_1c_2 should represent its solubility (24). The intersected points c_1 and c_2 were called the transition concentrations (C_{tr}) or invariant points, and they represent the concentration of reactants in solution when the solid phase at equilibrium contains cocrystal and MYR (or NIC) (25). Therefore, the PSD refers to the solution composition of MYR and NIC at equilibrium with different solid phases.

However, the reactant concentration in solution is not enough to achieve cocrystal preparation. Unlike the PSD, the TPD shows the total composition of the system, including components in the solid and liquid phases (20,26). Thus, the phase solubility curve should be transformed into the TPD (Fig. 3). Furthermore, a straight line was drawn to connect these two points (c_1, c_2) and a new region appeared, which was

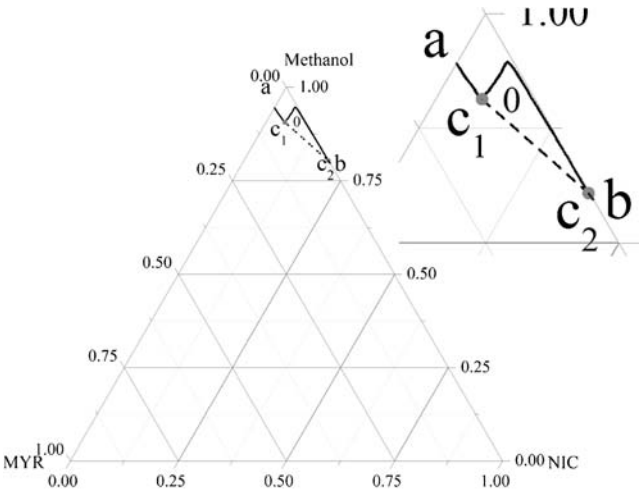

Fig. 3 The ternary phase diagram (TPD) was transformed from the PSD. The point in the TPD means the total amount of 100 g with MYR, CCF, and methanol. The crystallization of pure cocrystal forms in solution in region 0.

labeled region 0. According to the principles of a TPD, if a MYR/NIC/Methanol mixture is generated with a starting composition in region 0, pure solid MYR-NIC cocrystal would be precipitated from the system, and the liquid composition can be varied on the curved full line c_1c_2. Obviously, region 0 is within the pure cocrystal forming zone, which cannot be obtained without knowledge of the cocrystal composition. However, region 0 could be easily found by drawing the PSD; therefore, it was useful to cocrystal preparation when the cocrystal composition is unknown (27–29).

We selected a point lying within region 0 of the TPD and created a mixture with the overall composition of 2.0% (w/w) MYR, 6.7% (w/w) NIC, and 91.3% (w/w) methanol to prepare MYR-NIC cocrystals as mentioned in the "Preparation of Cocrystals" section. Using the same method, the other three MYR cocrystals were also obtained.

Solid-State Properties

DSC

The DSC curves of MYR, CCFs, and cocrystals are shown in Fig. 4, from which it can be seen that pure MYR presented a single sharp endothermic melting peak at 356.06°C (Fig. 4a). CAF demonstrated a steep endothermic melting transition at 236.29°C (Fig. 4c), which is in agreement with the reported thermal behavior (30). Meanwhile, the DSC thermogram for MYR-CAF cocrystals showed a single endothermic transition, which was attributed to the melting transition (275.01°C) with a melting enthalpy of 142 J/g (Fig. 4b); the melting temperature was markedly different than the endothermic melting peak of MYR or CAF, suggesting the formation of a new phase. The MYR-NIC, MYR-INM, MYR-CYA cocrystals, and their CCFs resulted in similar phenomena with MYR-CAF cocrystals and CAF. They melted at 214.46°C, 257.53°C, and 191.51°C, respectively, with a melting enthalpy of 160 J/g, 59 J/g, and 232 J/g (Fig. 4d, f, and h). A single endothermic transition for the four cocrystals demonstrates that the new phases were stable below their melting points and indicates the absence of unbound or absorbed solvent and water (31).

Furthermore, a direct correlation of chemical structure to the crystalline lattice energy and melting point is a challenging task because of several contributing factors, such as molecular arrangement in the lattice, noncovalent interactions, and conformational flexibility for a molecule (31), and this becomes more complex with cocrystals with multiple components. In the current study, an interesting pattern was found in that the melting points of all cocrystals were between that of MYR and the corresponding CCF, which is in agreement with the universal rule obtained from other cocrystals (32,33). It is clear that the melting point of the cocrystals was altered with the type of CCF. This information suggests that CCFs with higher

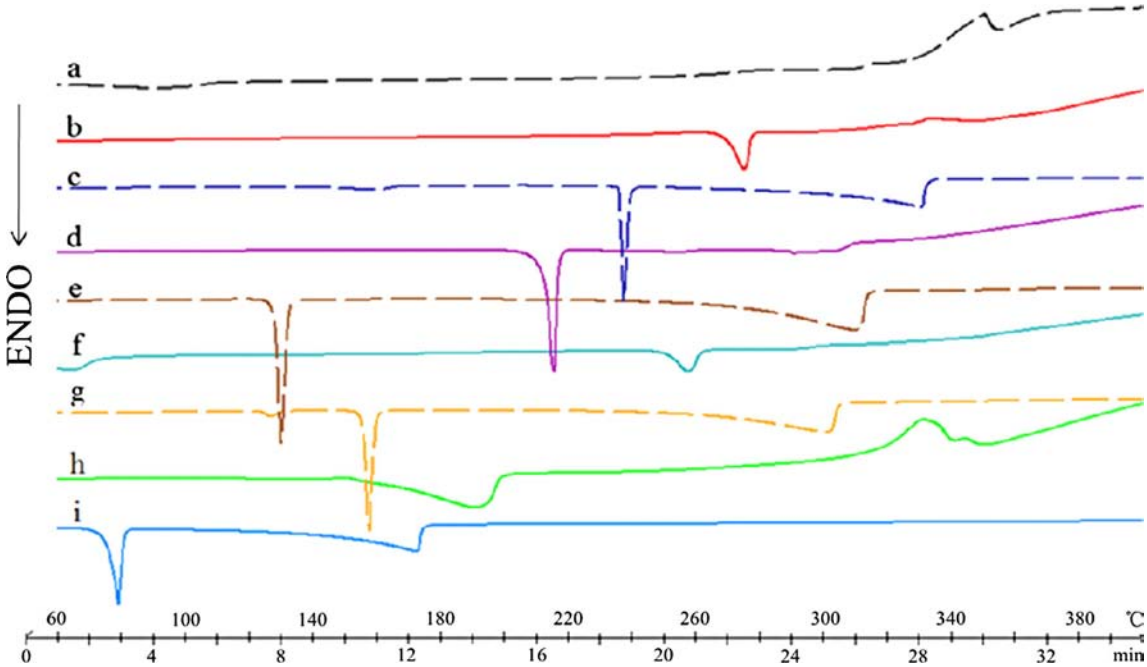

Fig. 4 DSC results of pure MYR (**a**), MYR-CAF cocrystal (**b**), pure CAF (**c**), MYR-NIC cocrystal (**d**), pure NIC (**e**), MYR-INM cocrystal (**f**), pure INM (**g**), MYR-CYA cocrystal (**h**), and pure CYA (**i**) with heating at 10°C/min.

melting points should be selected if MYR cocrystals with higher melting points are desired.

PXRD

The PXRD patterns of MYR, CCFs, and their cocrystals are shown in Fig. 5. The PXRD patterns of the four cocrystals clearly differed from those of the individual API and CCF, indicating the presence of a new crystalline phase. Specifically, several new reflections (marked with black triangles in Fig. 5) were observed; however, various characteristic reflections of MYR and the CCFs were absent. Taking the MYR-CAF cocrystals as an example, they exhibited some new characteristic reflections at 2θ 10.76°, 12.32°, 17.94°, 18.30°, and 21.94° (Fig. 5b), which allowed the MYR-CAF cocrystal to be distinguished from MYR and CAF. In addition, 2θ angles like 7.52°, 9.10°, 15.78°, 26.08°, 39.56°, 40.38°, 41.38°, and 46.62° of MYR (Fig. 5a) and 11.93°, 20.52°, 23.62°, 36.38°, and 44.26° of CAF (Fig. 5c) could not be observed in the powder pattern of the MYR-CAF cocrystals.

FT-IR

IR spectroscopy is a reliable technique to characterize hydrogen bonding because a change in hydrogen bonds at the intermolecular level results in distinct vibrational frequency shifts.

As shown in Fig. 6a, MYR showed peaks at 3,415 cm^{-1} (corresponding to O-H stretching vibrations), 1,663 cm^{-1} and 1,618 cm^{-1} (-C = O stretching vibrations), 1,554 cm^{-1} (C = C stretching vibrations), 1,520 cm^{-1} (aromatic group), 1,326 cm^{-1} and 1,168 cm^{-1} (C–O–C vibrations), and 1,028 cm^{-1} (C–H bending vibrations). The four cocrystals (Fig. 6b, d, f, and h) showed distinct shifts in the hydroxyl and carbonyl region of MYR, which implied that the O-H group and C = O group in MYR were likely participating in the formation of hydrogen bonds in the cocrystallization process. For example, the O-H and C = O stretching frequency of the MYR-NIC cocrystal shifted from their original positions in MYR to 3,470 cm^{-1} and 1,661 cm^{-1}, respectively.

The four CCFs have the same chemical group, a N-containing heterocyclic ring, in which the N atom is a competitive acceptor (34). The C = N stretch shifts from 1,619, 1,624, 1,658, 1,593 cm^{-1} in NIC, INM, CAF, and CYA, respectively, to 1,606, 1,603, 1,646, 1,570 cm^{-1} in their corresponding cocrystals, which implies that the N-containing heterocyclic rings in the four CCFs participate in strong hydrogen bonds in the cocrystallization process. In addition, the C = O stretching vibrations shifted from 1,681, 1,664, and 1,700 cm^{-1} in NIC, INM, and CAF to larger wavenumbers (1,685, 1,686, and 1,705 cm^{-1}) in their corresponding cocrystals, indicating that the carbonyl stretching vibrations of the amide groups was another characteristic for the formation of hydrogen bonds in MYR-NIC, MYR-INM, and MYR-CAF cocrystals. The phenomena also means that higher energies are required for stretching the C = O bonds

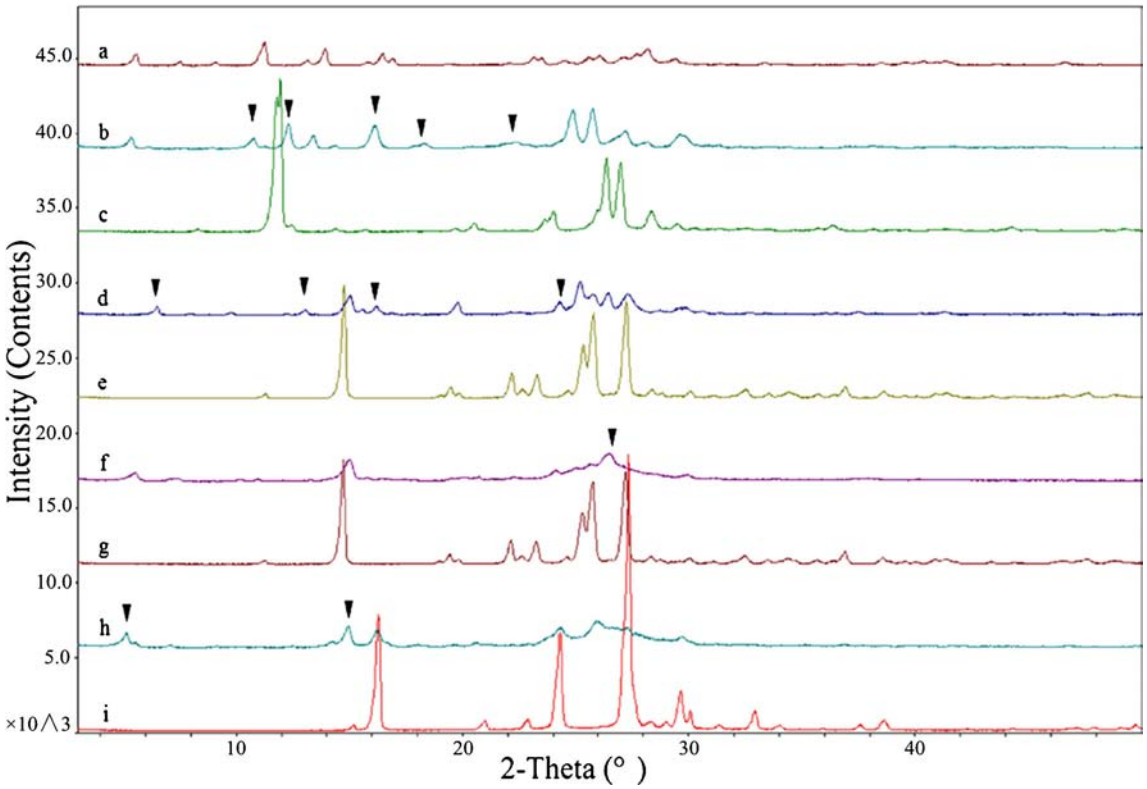

Fig. 5 PXRD patterns of pure MYR (**a**), MYR-CAF cocrystal (**b**), pure CAF (**c**), MYR-NIC cocrystal (**d**), pure NIC (**e**), MYR-INM cocrystal (**f**), pure INM (**g**), MYR-CYA cocrystal (**h**), and pure CYA (**i**).

when the CCFs are embedded in cocrystals (35). Differently, the IR vibrational modes corresponding to –CN in CYA were changed from 2,242 to 2,237 cm^{-1} in the MYR-CYA cocrystals, indicating the formation of a new supramolecular synthon –CN…H-O- in the cocrystals (36).

Thus, the variations obtained from comparing the spectra of the four MYR cocrystals with those of the starting components suggest that the cocrystals of MYR and the CCFs were formed with various hydrogen bonds.

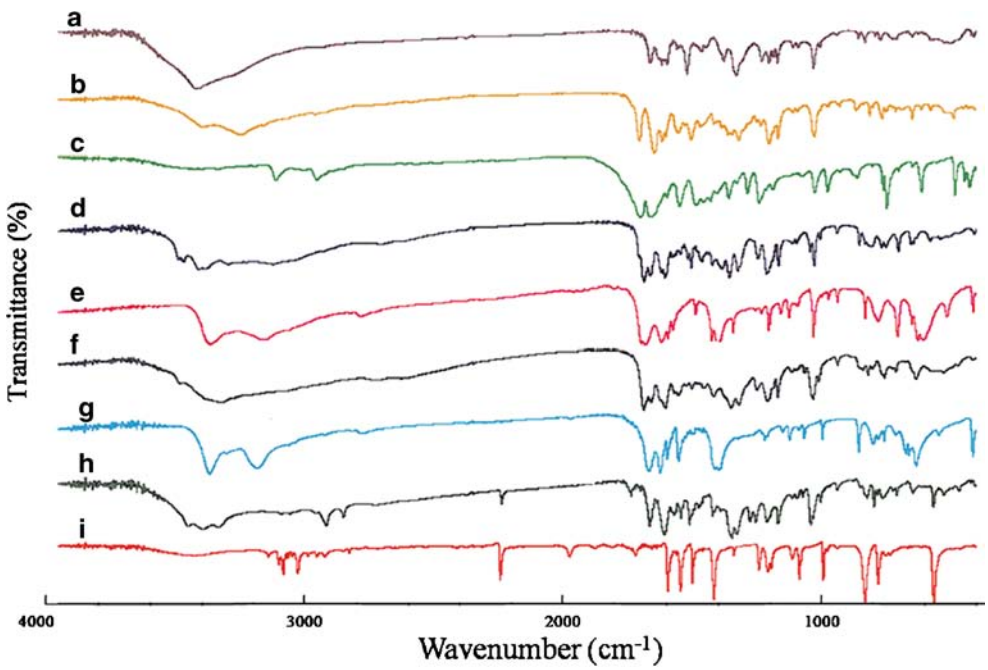

Fig. 6 FTIR results of pure MYR (**a**), MYR-CAF cocrystal (**b**), pure CAF (**c**), MYR-NIC cocrystal (**d**), pure NIC (**e**), MYR-INM cocrystal (**f**), pure INM (**g**), MYR-CYA cocrystal (**h**), and pure CYA (**i**).

SEM

The SEM results of MYR and its four cocrystals are presented in Fig. 7. As shown in Fig. 7a, the particle size of MYR is approximately 50 μm and its shape is always needle-like. However, the MYR-CAF, MYR-NIC, and MYR-INM cocrystals showed a smaller particle size ranging from 2 to 10 μm (Fig. 7b, c, and d). In addition, the MYR-CAF and MYR-NIC cocrystals exhibited a clear rod-like morphology, whereas the MYR-INM cocrystals exhibited block particles with a smooth surface. However, as shown in Fig. 7e, the MYR-CYA cocrystals crystallized in large block particles with many crystal features, such as rough surfaces and irregular edges. The diameter of the blocks ranged from 10 to 100 μm. The morphology of the particles revealed marked differences between MYR and the four synthesized cocrystals, which indicates that different crystal forms have been obtained.

NMR

Solution ^{1}H-NMR was used to identify and confirm the ratio of MYR and the coformer in each cocrystal system. Three different stoichiometric cocrystals were formed, MYR-CAF (1:1), MYR-NIC (1:2), MYR-INM (1:2), and MYR-CYA (1:3) (Fig. 8), according to the ratio of the characteristic peak area of the API and CCF in the cocrystals (37).

TPD and Verification

As previously stated, MYR and NIC crystallized with a 1:2 molar ratio in the MYR-NIC cocrystal. Converting this mole fraction to a mass fraction, a new point was obtained on the horizontal axis of the TPD (Fig. 9), which was labeled as point d, and this point is a constant value and does not change with solution composition (14). Point a is the solubility of MYR and point b is the solubility of NIC in neat methanol, and the values are 5.4% (w/w) and 20.2% (w/w), respectively. The c_1d, c_2d, c_1MYR, and c_2NIC points were connected, which meant the intact TPD of the MYR-NIC-Methanol system at 25°C was completed. In the TPD shown in Fig. 9, region 1 is the solution phase where the system is under-saturated with no solid at equilibrium. Regions 2 and 6 are the stable regions of pure solid MYR and NIC, respectively. The presence of NIC in methanol decreases the solubility of MYR to 5.0% (w/w) (ac_1), which suggests a complex formation between the two components in dilute solutions (19). In contrast, the solubility of NIC always fluctuates around 20% (w/w) by the addition of MYR, which can be more clearly observed in the PSD (Fig. 2) and implies little change in the relative strengths of the intermolecular interactions. The reasonable explanation is that MYR is so weakly solvated by methanol (45 mg/mL) that the presence of a second solute with strong H-bonding ability would have a significant effect on its solubility. However, NIC is already solvated by methanol (201 mg/mL); therefore, its solubility is not greatly affected by the addition of MYR (38).

In region 3, the solid phases of pure MYR and the 1:2 cocrystal are in equilibrium with a solution of invariant composition c_1, whereas solid NIC and the cocrystal are at equilibrium with that of c_2 in region 5. Pure 1:2 cocrystals in equilibrium with a solution of MYR and NIC is in region 4, from which we can clearly see the previous region 0 in Fig. 3 has been expanded to region 4; therefore, our strategy for

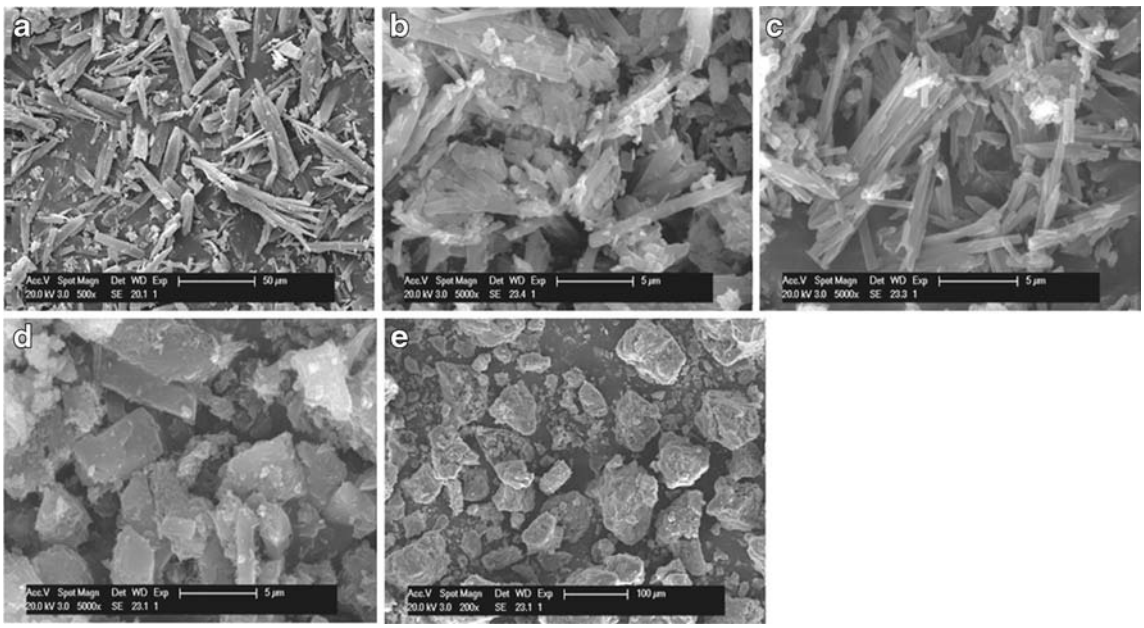

Fig. 7 SEM results of MYR and cocrystals. The differences between MYR and the four cocrystals in crystal quality (shape, surface, and size) are shown in pure MYR (**a**), MYR-CAF cocrystal (**b**), MYR-NIC cocrystal (**c**), MYR-INM cocrystal (**d**), and MYR-CYA cocrystal (**e**).

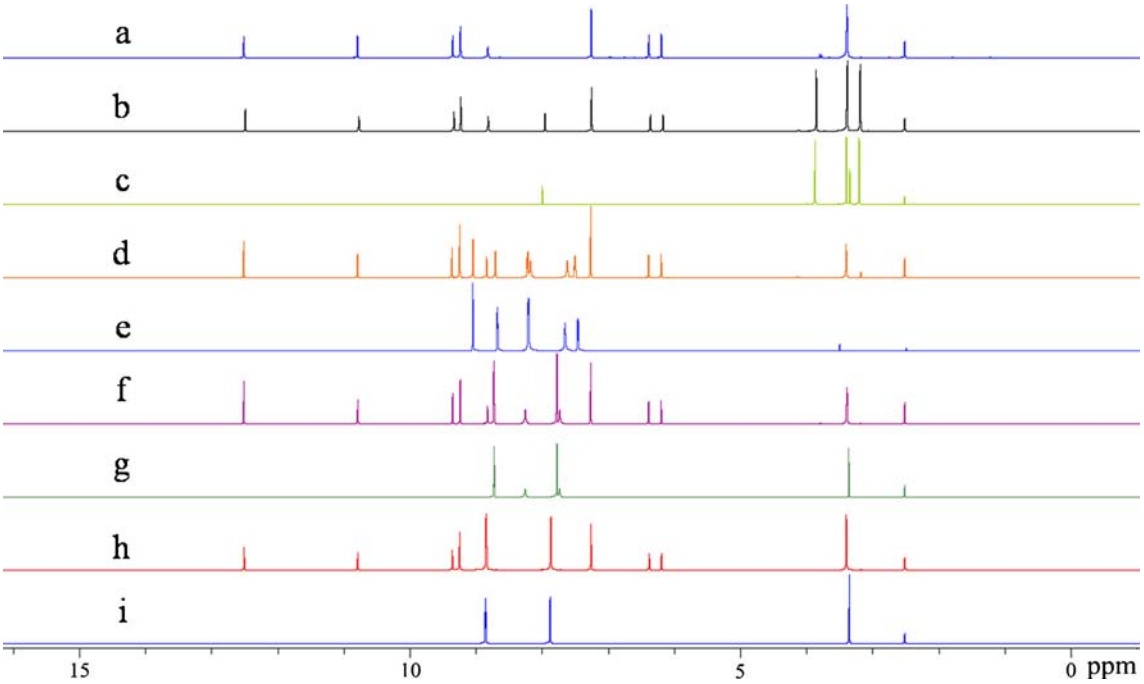

Fig. 8 Solution ^{1}H-NMR patterns of samples to identify and confirm the ratio of MYR and CCFs in each cocrystal system: (**a**) pure MYR, (**b**) MYR-CAF cocrystal, (**c**) pure CAF, (**d**) MYR-NIC cocrystal, (**e**) pure NIC, (**f**) MYR-INM cocrystal, (**g**) pure INM, (**h**) MYR-CYA cocrystal, and (**i**) pure CYA.

preparing pure cocrystals is credible. However, these viewpoints are based on the precondition that our constructed TPD is exactly correct. Therefore, we have made an effort to prove the rationality of the TPD in the following works.

On one hand, the most direct way was performed by choosing the point in the drawn TPD randomly and then characterizing the solid phases after the reaction. Figure 9 shows the position of the selected points, and Figs. 10 and 11 separately give the DSC and PXRD analysis of the solid phases obtained from the different experimental conditions

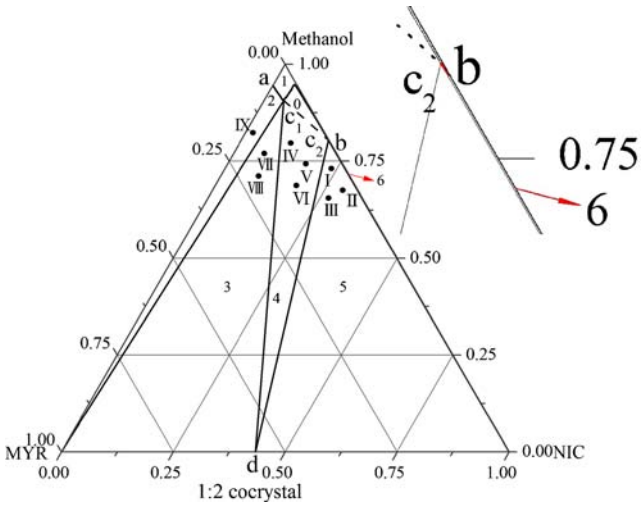

Fig. 9 The ternary phase diagram of MYR-NIC-Methanol at 25°C in mass percent: (**1**) liquids, (**2**) MYR + liquid, (**3**) MYR + cocrystal + liquid, (**4**) cocrystal + liquid, (**5**) NIC + cocrystal + liquid, and (**6**) NIC + liquid. The *black points* were selected for TPD verification.

at equilibrium. Samples I, II, and III were prepared using ratios of API to CCF to solvent that correspond to a region of the TPD where at equilibrium both cocrystal and NIC would be expected to be present as solid phases. DSC analysis of solid phases I, II, and III (Fig. 10) demonstrated that these samples did indeed contain both cocrystal and NIC as melting events were observed at about 130°C and 215°C, respectively. However, the second peaks in solid phases I and II did not match the temperature of melting of cocrystal (214.46°C) in Fig. 4d and the similar situation happened in the curves of solid phases VII and VII, which should be the mixture of cocrystal and MYR. The probable explanation might be that the DSC process of a physical mixture like cocrystal with API or CCF was comparatively complicated so that some characteristic peaks would shift with the change of the ratios of cocrystal and CCF/MYR in the mixture or the cocrystal formation kinetics (39). Fortunately, the results of PXRD patterns of solid phases I, II, III, VII, and VII demonstrated that these samples did contain both cocrystal and NIC or MYR because both of their characteristic reflections (marked with red circles in Fig. 11) were observed. In addition, the DSC and PXRD patterns of the rest points (IV, V, VI, IX) perfectly matched with the predicted results from the TPD.

On the other hand, the C_{tr} was used for the verification because the two invariant points are critical indicators of cocrystal solubility and stability domains (40). First, the prediction of the phase transformations and determination of the thermodynamic stability of individual cocrystal systems are both closely related to the C_{tr} (22). Second, the C_{tr} can be used to determine cocrystal solubility, particularly

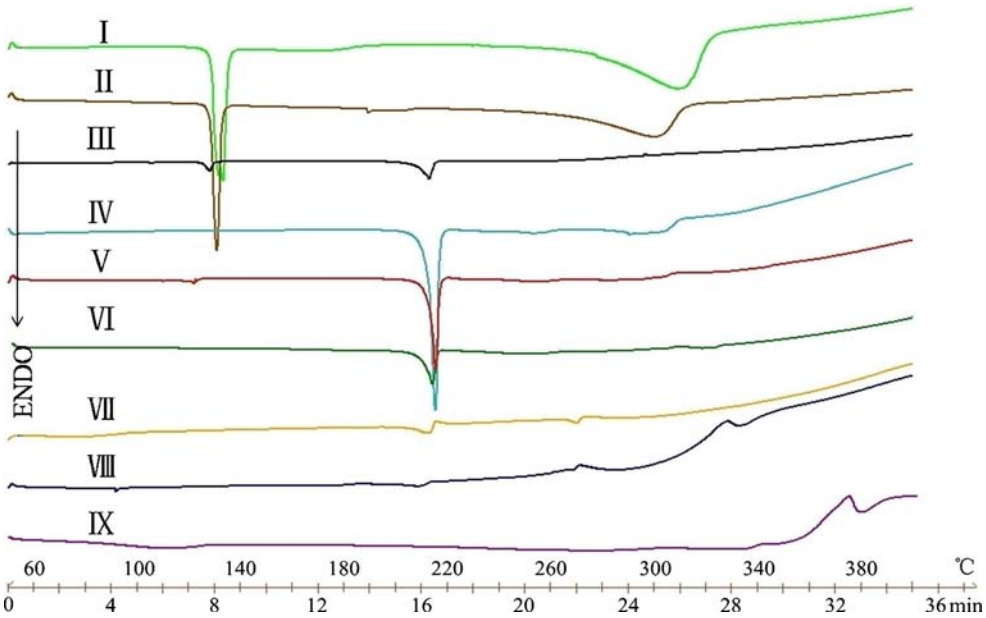

Fig. 10 The DSC results of solid phases at equilibrium. The sample (**I**, **II**, **III**, **IV**, **V**, **VI**, **VII**, **VII**, **IX**) corresponds to the *black points* in the TPD, respectively.

for incongruently saturating cocrystals (metastable cocrystals) because the drug going into solution can be followed by crystallization in a supersaturable system (41–43). Lastly, knowing the critical points c_1, c_2, and d could accurately determine the main body of the critical region in the TPD (14), indicating that these three points are critical for the TPD construction. However, point d is fixed by the cocrystal composition. Thus, the other two points (c_1 and c_2) need to be validated using traditional methods. The results showed that two solid phases coexisted and the concentrations in solution (0.97±0.08 mg/mL of MYR and 191.44±0.44 mg/mL of NIC for c_1, 35.64±0.24 mg/mL of MYR and 41.08±0.12 mg/mL of NIC for c_2) were close to the predicted values (0.93 mg/mL of MYR and 191.32 mg/mL of NIC for c_1, 36.18 mg/mL of MYR and 41.69 mg/mL of NIC for c_2) at equilibrium, which confirmed that c_1 and c_2 were actually the

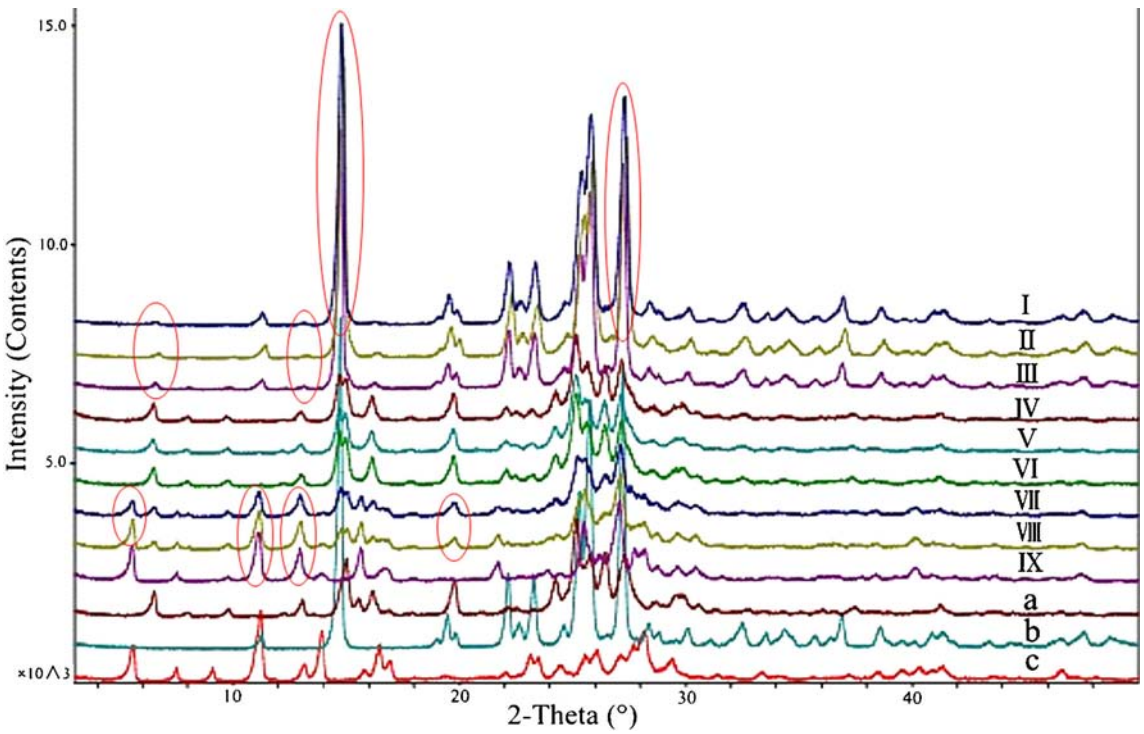

Fig. 11 The PXRD results of solid phases at equilibrium and MYR-NIC cocrystal (**a**), pure NIC (**b**), pure MYR (**c**). The sample (**I**, **II**, **III**, **IV**, **V**, **VI**, **VII**, **VII**, **IX**) corresponds to the *black points* in the TPD, respectively.

C_{tr} points. These two experiments validated that our strategy for cocrystal formation was reasonable.

Here, we introduced a novel strategy for cocrystal formation. First, the PSD of MYR and CCF was constructed, from which the reactant concentrations in solution at equilibrium were obtained, and the change process of the phases was predicted. Second, by transforming the curve in the PSD to a TPD, a new region was obtained, which could guide us to prepare pure cocrystals. Third, after determining the composition of the prepared cocrystal by NMR, the TPD of the API-CCF-Solvent system was constructed.

The strategy has several advantages: (1) powder cocrystals could be prepared without knowledge of the stoichiometric ratio; therefore, this method could overcome the shortage of the fixed stoichiometric ratio in previous cocrystal research; (2) the TPD of the API-CCF-Solvent system was constructed by combining the constructed PSD and NMR data before the pure cocrystal was obtained, which was convenient and different from the traditional method; (3) cocrystal preparation and the TPD construction were simultaneously performed, indicating that this strategy was an efficient and economic measure for cocrystal research. However, similar to the other cocrystal research methods, it has its limitations. For example, the fact that the cocrystal of the drug and CCF could be definitively formed in the selected solvent was a precondition of this strategy. Furthermore, this strategy is not suitable for cocrystals with two or more stoichiometric ratios of API and CCF in the same solvent and temperature because there could be three or more invariant points under that condition, which would make it difficult to determine their accurate positions in the TPD. Therefore, to further optimize the strategy and simultaneously overcome these limitations as well as enlarge the method's applicable scope is a critical issue and needs to be further investigated.

Powder Dissolution Studies

The powder dissolution profiles for the four cocrystals and pure MYR were obtained from the slurry experiments performed in three different pH buffers, which were used to evaluate the drug dissolution rate in different physiological environments (44). From the dissolution profiles (Fig. 12), the four cocrystals displayed an increased solubility and dissolution rate than MYR in each media; thus, the solubility of MYR in cocrystals was increased by approximately 3–80 fold and the time to reach the maximum value was decreased to only 10–20 min. In fact, the highest solubility of MYR exhibited by the MYR-CAF, MYR-NIC, MYR-INM, and MYR-CAY cocrystals in three media were enhanced from less than 1.5 μg/mL in the crude MYR to 11.9 μg/mL, 10.9 μg/mL, 9.8 μg/mL, and 7.1 μg/mL, respectively, which implies that cocrystallization is an effective approach for improving the solubility of MYR.

As shown in Fig. 12, the solubility of MYR in pH 4.5 acetate buffer is approximately 1.5 μg/mL, whereas it is nearly insoluble in 0.1 M HCl and pH 6.8 phosphate buffer, which suggests that the solubility of MYR is pH dependent in aqueous buffer. Similar to MYR, the four MYR cocrystals had increased solubility in pH 4.5 acetate buffer. All cocrystals exhibited higher solubility and reached maximum solubility more quickly than in the other two mediums. Here, the pH-dependent phenomenon of each MYR cocrystal might be dominated by the API (MYR), and the similar results were obtained in other cocrystals, such as carbamazepine-saccharin cocrystals (45), acyclovir-glutaric acid cocrystals (46), adefovir dipivoxil-saccharin cocrystals (44), and indomethacin-saccharin cocrystals (42).

However, in the same dissolution media, the solubility of a cocrystal might follow the CCF solubility rule (47); i.e., a high solubility CCF imparts a high solubility on the cocrystal. A good correlation between the solubility of the MYR cocrystals and their corresponding CCF in each media could be observed from Fig. 12 and SciFinder data. For example, the order of cocrystal solubility in pH 4.5 acetate buffer is: MYR-CAF > MYR-NIC > MYR-INM > MYR-CYA, which was consistent with the solubility order obtained from SciFinder, CAF (58 g/L) > NIC (53 g/L) > INM (45 g/L) > CYA (12 g/L). Thus, the CCF solubility rule was embodied in the four different MYR cocrystals. Other pharmaceutical cocrystals, such as pyrazinecarboxamide with various carboxylic acids and febuxostat with 5 pharmaceutically acceptable CCFs, followed the CCF solubility rule on their dissolution and solubility results (48,49).

Interestingly, several MYR cocrystals showed a slightly secondary peak concentration at approximately 120 min. The phenomenon might be explained by the dissociation of cocrystals into their components, which was attributed to weak intermolecular forces in the cocrystals (41). In general, during the dissolution process, the neat cocrystals transformed rapidly to the low-soluble drug (MYR), and MYR became supersaturated and immediately crystallized as the single-component MYR. Therefore, the high solubility of the four MYR cocrystals is not likely the maximum values, which were enhanced by the cocrystal technology. Supersaturation is a common phenomenon in many cocrystal dissolution experiments (40,50), which greatly confines the role of cocrystals in enhancing the solubility of insoluble drugs. Currently, the measures to solve the problem are mainly focused on the following two points: one is to calculate the solubility of cocrystals with the C_{tr}, which has been mentioned in the "TPD and Verification" section (41–43) and to choose the most suitable cocrystals from the results; the other method is to design a formulation of cocrystals with the aim of controlling the supersaturation levels (51). As far as the present study was concerned, whether the dissociation of cocrystals into the poorly soluble drug (MYR) and CCFs during dissolution

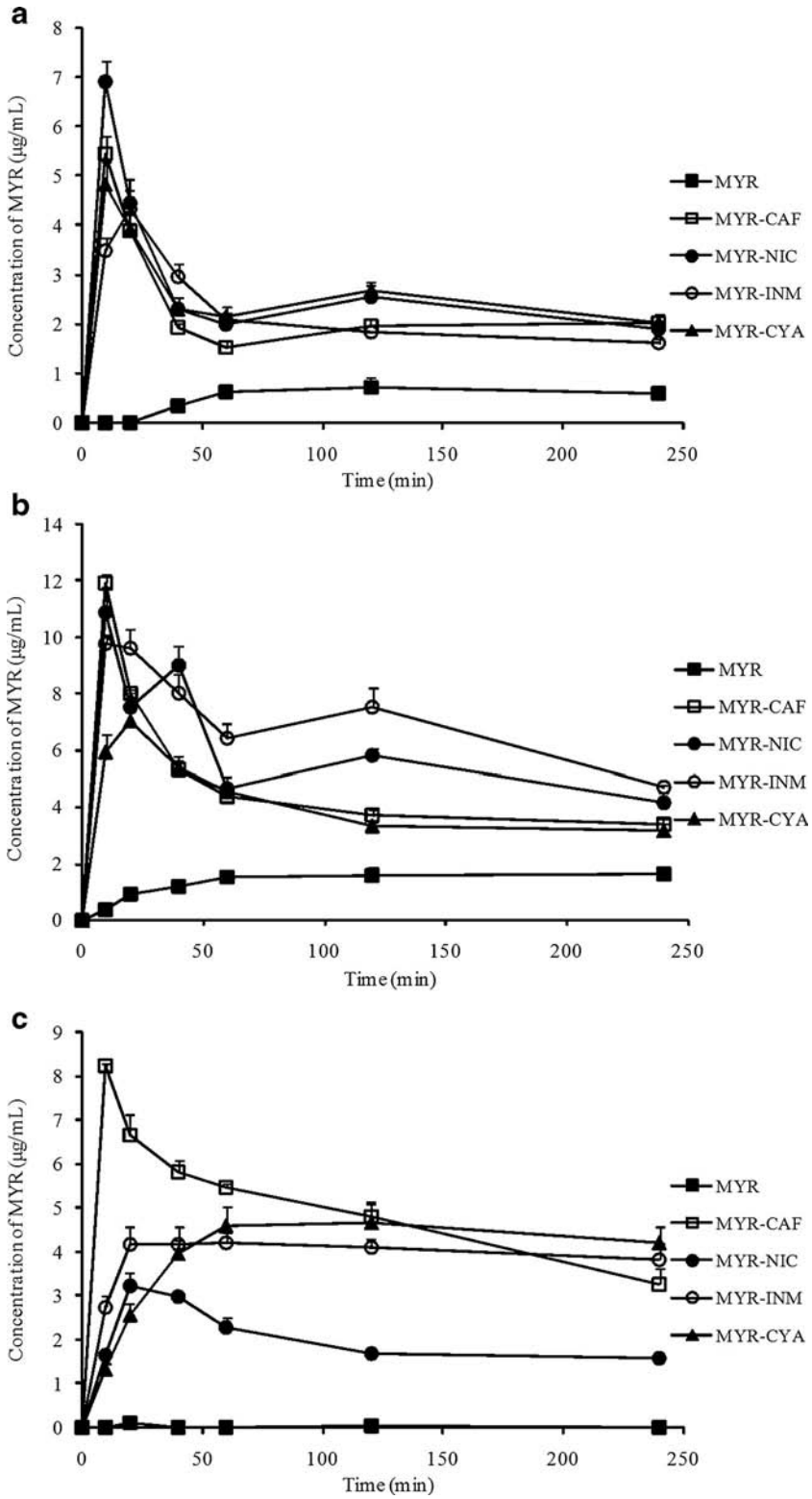

Fig. 12 Powder dissolution profile of MYR and its four cocrystals in 0.1 M HCl aqueous solution (**a**), pH 4.5 acetate buffer (**b**), and pH 6.8 phosphate buffer (**c**).

could be avoided by the above mentioned approaches is unknown and worth future study.

In short, MYR cocrystals present a pH-dependent dissolution profile and exhibit a complete and rapid dissolution in all experimental aqueous media compared to pure MYR, which is probably because of crystal packing and the process of cocrystallization. From this research, it can be concluded that cocrystals provide a new approach for dissolution enhancement

by forming intermolecular hydrogen bonding between MYR and CCF, which offers opportunities for MYR to be therapeutic agents.

CONCLUSION

Pharmaceutical cocrystals of MYR with CAF, NIC, INM, and CYA were successfully prepared and characterized by DSC, PXRD, IR, SEM, and NMR. A novel strategy for cocrystal preparation without knowledge of the stoichiometric ratio based on the TPD principle was developed. First, the PSD of MYR and CCF was constructed and was transformed into a TPD. Second, two invariant points were inferred and a part of the cocrystal forming region was obtained, which guided us in preparing pure cocrystal. Third, the TPD of the API-CCF-solvent system was completely constructed by determining the composition of the cocrystal by NMR. In addition, the dissolution results demonstrate that the solubility and dissolution rates of MYR were significantly improved by cocrystallization with the four CCFs, and all cocrystals exhibited pH-dependent solubility.

ACKNOWLEDGMENTS AND DISCLOSURES

This study was sponsored by the National Science Foundation of China (81303304), the Innovation Program of the Shanghai Municipal Education Commission (14YZ057), the Specialized Research Fund for the Doctoral Program of Higher Education (20133107120006), and the Nano-specific Project of the Shanghai Science and Technology Commission (12 nm0502400).

REFERENCES

1. Eddleston MD, Sivachelvam S, Jones W. Screening for polymorphs of cocrystals: a case study. Cryst Eng Comm. 2013;15(1):175–81.
2. Qiao N, Li MZ, Schlindwein W, Malek N, Davies A, Trappitt G. Pharmaceutical cocrystals: an overview. Int J Pharm. 2011;419(1–2):1–11.
3. Seliger J, Zagar V. Nuclear quadrupole resonance characterization of carbamazepine cocrystals. Solid State Nucl Magn Reson. 2012;47–48(1):47–52.
4. Yamamoto K, Tsutsumi S, Ikeda Y. Establishment of cocrystal cocktail grinding method for rational screening of pharmaceutical cocrystals. Int J Pharm. 2012;437(1–2):162–71.
5. Lipinski CA. Drug-like properties and the causes of poor solubility and poor permeability. J Pharmacol Toxicol Methods. 2000;44(1):235–49.
6. Ong KC, Khoo HE. Biological effects of myricetin. Gen Pharmacol Vasc Sys. 1997;29(2):121–6.
7. Scheidt HA, Pampel A, Nissler L, Gebhardt R, Huster D. Investigation of the membrane localization and distribution of flavonoids by high-resolution magic angle spinning NMR spectroscopy. Biochim Biophys Acta. 2004;1663(1–2):97–107.
8. Kim H, Choi J, Jung S. Inclusion complexes of modified cyclodextrins with some flavonols. J Incl Phenom Macrocycl Chem. 2009;64(1–2):43–7.
9. Mira L, Fernandez MT, Santos M, Rocha R, Florencio MH, Jennings KR. Interactions of flavonoids with iron and copper ions: a mechanism for their antioxidant activity. Free Radic Res. 2002;36(11):1199–208.
10. Roedig-Penman A, Gordon MH. Antioxidant properties of myricetin and quercetin in oil and emulsions. J Am Oil Chem Soc. 1998;75(2):169–80.
11. Ma ZG, Liu TW. Myricetin facilitates potassium currents and inhibits neuronal activity of PVN neurons. Neurochem Res. 2012;37(7):1450–6.
12. Yao YS, Lin GB, Xie Y, Ma P, Li GW, Meng QC, *et al.* Preformulation studies of myricetin: a natural antioxidant flavonoid. Die Pharm. 2014;69(1):19–26.
13. Variankaval N, Wenslow R, Murry J, Hartman R, Helmy R, Kwong E, *et al.* Preparation and solid-state characterization of nonstoichiometric cocrystals off a phosphodiesterase-IV inhibitor annul L-tartaric acid. Cryst Growth Des. 2006;6(3):690–700.
14. Leung DH, Lohani S, Ball RG, Canfield N, Wang YL, Rhodes T, *et al.* Two novel pharmaceutical cocrystals of a development compound–screening, scale-up, and characterization. Cryst Growth Des. 2012;12(3):1254–62.
15. Arenas-Garcia JI, Herrera-Ruiz D, Mondragon-Vasquez K, Morales-Rojas H, Hopfl H. Modification of the supramolecular hydrogen-bonding patterns of acetazolamide in the presence of different cocrystal formers: 3:1, 2:1, 1:1, and 1:2 cocrystals from screening with the structural isomers of hydroxybenzoic acids, aminobenzoic acids, hydroxybenzamides, aminobenzamides, nicotinic acids, nicotinamides, and 2,3-dihydroxybenzoic acids. Cryst Growth Des. 2012;12(2):811–24.
16. Ando S, Kikuchi J, Fujimura Y, Ida Y, Higashi K, Moribe K, *et al.* Physicochemical characterization and structural evaluation of a specific 2:1 cocrystal of naproxen-nicotinamide. J Pharm Sci. 2012;101(9):3214–21.
17. Gangopadhyay P, Radhakrishnan TP. Visualizing supramolecular macrocyclic formations. Mol Cryst Liq Cryst. 2001;369(1):167–219.
18. Yenikaya C, Ogretir C. A quantum chemical study on structure of cocrystal of triphenylphosphine oxide and hydroquinone. J Mol Struct THEOCHEM. 2005;731(1–3):1–5.
19. Jayasankar A, Reddy LS, Bethune SJ, Rodriguez-Hornedo N. Role of cocrystal and solution chemistry on the formation and stability of cocrystals with different stoichiometry. Cryst Growth Des. 2009;9(2):889–97.
20. Chiarella RA, Davey RJ, Peterson ML. Making co-crystals–the utility of ternary phase diagrams. Cryst Growth Des. 2007;7(7):1223–6.
21. Rodriguez-Hornedo N, Nehru SJ, Seefeldt KF, Pagan-Torres Y, Falkiewicz C. Reaction crystallization of pharmaceutical molecular complexes. Mol Pharm. 2006;3(3):362–7.
22. Good DJ, Rodriguez-Hornedo N. Cocrystal eutectic constants and prediction of solubility behavior. Cryst Growth Des. 2010;10(3):1028–32.
23. Nehm SJ, Rodriguez-Spong B, Rodriguez-Hornedo N. Phase solubility diagrams of cocrystals are explained by solubility product and solution complexation. Cryst Growth Des. 2006;6(2):592–600.
24. Zhang S, Rasmuson AC. Thermodynamics and crystallization of the theophylline-glutaric acid cocrystal. Cryst Growth Des. 2013;13(3):1153–61.
25. Grossjohann C, Eccles KS, Maguire AR, Lawrence SE, Tajber L, Corrigan OI, *et al.* Characterisation, solubility and intrinsic dissolution behaviour of benzamide: dibenzyl sulfoxide cocrystal. Int J Pharm. 2012;422(1–2):24–32.

26. Childs SL, Rodriguez-Hornedo N, Reddy LS, Jayasankar A, Maheshwari C, McCausland L, *et al.* Screening strategies based on solubility and solution composition generate pharmaceutically acceptable cocrystals of carbamazepine. Cryst Eng Comm. 2008;10(7):856–64.
27. Ainouz A, Authelin JR, Billot P, Lieberman H. Modeling and prediction of cocrystal phase diagrams. Int J Pharm. 2009;374(1–2):82–9.
28. Croker DM, Foreman ME, Hogan BN, Maguire NM, Elcoate CJ, Hodnett BK, *et al.* Understanding the p-toluenesulfonamide/triphenylphosphine oxide crystal chemistry: a new 1:1 cocrystal and ternary phase diagram. Cryst Growth Des. 2012;12(2):869–75.
29. Seaton CC, Parkin A, Wilson CC, Blagden N. Controlling the formation of benzoic acid: isonicotinamide molecular complexes. Cryst Growth Des. 2009;9(1):47–56.
30. Eddleston MD, Lloyd GO, Jones W. Cocrystal dissociation and molecular demixing in the solid state. Chem Commun. 2012;48(65):8075–7.
31. Vangala VR, Chow PS, Tan RBH. Co-crystals and co-crystal hydrates of the antibiotic nitrofurantoin: structural studies and physicochemical properties. Cryst Growth Des. 2012;12(12):5925–38.
32. Schultheiss N, Newman A. Pharmaceutical cocrystals and their physicochemical properties. Cryst Growth Des. 2009;9(6):2950–67.
33. Stanton MK, Bak A. Physicochemical properties of pharmaceutical co-crystals: a case study of ten AMG 517 co-crystals. Cryst Growth Des. 2008;8(10):3856–62.
34. Weyna DR, Shattock T, Vishweshwar P, Zaworotko MJ. Synthesis and structural characterization of cocrystals and pharmaceutical cocrystals: mechanochemistry vs. slow evaporation from solution. Cryst Growth Des. 2009;9(2):1106–23.
35. Espinosa-Lara JC, Guzman-Villanueva D, Arenas-Garcia JI, Herrera-Ruiz D, Rivera-Islas J, Roman-Bravo P, *et al.* Cocrystals of active pharmaceutical ingredients-praziquantel in combination with oxalic, malonic, succinic, maleic, fumaric, glutaric, adipic, and pimelic acids. Cryst Growth Des. 2013;13(1):169–85.
36. Mohamed S, Tocher DA, Price SL. Computational prediction of salt and cocrystal structures-does a proton position matter? Int J Pharm. 2011;418(2):187–98.
37. Alhalaweh A, George S, Basavoju S, Childs SL, Rizvi SAA, Velaga SP. Pharmaceutical cocrystals of nitrofurantoin: screening, characterization and crystal structure analysis. Cryst Eng Comm. 2012;14(15):5078–88.
38. Guo K, Sadiq G, Seaton C, Davey R, Yin QX. Co-crystallization in the caffeine/maleic acid system: lessons from phase equilibria. Cryst Growth Des. 2010;10(1):268–73.
39. Yamashita H, Hirakura Y, Yuda M, Teramura T, Terada K. Detection of cocrystal formation based on binary phase. Pharm Res. 2013;30(1):70–80.
40. Thakuria R, Delori A, Jones W, Lipert MP, Roy L, Rodriguez-Hornedo N. Pharmaceutical cocrystals and poorly soluble drugs. Int J Pharm. 2013;453(1):101–25.
41. Bethune SJ, Huang N, Jayasankar A, Rodriguez-Hornedo N. Understanding and predicting the effect of cocrystal components and pH on cocrystal solubility. Cryst Growth Des. 2009;9(9):3976–88.
42. Alhalaweh A, Roy L, Rodriguez-Hornedo N, Velaga SP. pH-dependent solubility of indomethacin-saccharin and carbamazepine-saccharin cocrystals in aqueous media. Mol Pharm. 2012;9(9):2605–12.
43. Reddy LS, Bethune SJ, Kampf JW, Rodriguez-Hornedo N. Cocrystals and salts of gabapentin: pH dependent cocrystal stability and solubility. Cryst Growth Des. 2009;9(1):378–85.
44. Gao YA, Zu H, Zhang JJ. Enhanced dissolution and stability of adefovir dipivoxil by cocrystal formation. J Pharm Pharmacol. 2011;63(4):483–90.
45. Rahman Z, Samy R, Sayeed VA, Khan MA. Physicochemical and mechanical properties of carbamazepine cocrystals with saccharin. Pharm Dev Technol. 2012;17(4):457–65.
46. Bruni G, Maietta M, Maggi L, Mustarelli P, Ferrara C, Berbenni V, *et al.* Preparation and physicochemical characterization of acyclovir cocrystals with improved dissolution properties. J Pharm Sci. 2013;102(11):4079–86.
47. Bolla G, Sanphui P, Nangia A. Solubility advantage of tenoxicam phenolic cocrystals compared to salts. Cryst Growth Des. 2013;13(5):1988–2003.
48. Maddileti D, Jayabun SK, Nangia A. Soluble cocrystals of the xanthine oxidase inhibitor febuxostat. Cryst Growth Des. 2013;13(7):3188–96.
49. Luo YH, Sun BW. Pharmaceutical co-crystals of pyrazinecarboxamide (PZA) with various carboxylic acids: crystallography, hirshfeld surfaces, and dissolution study. Cryst Growth Des. 2013;13(5):2098–106.
50. Shiraki K, Takata N, Takano R, Hayashi Y, Terada K. Dissolution improvement and the mechanism of the improvement from cocrystallization of poorly water-soluble compounds. Pharm Res. 2008;25(11):2581–92.
51. Childs SL, Kandi P, Lingireddy SR. Formulation of a danazol cocrystal with controlled supersaturation plays an essential role in improving bioavailability. Mol Pharm. 2013;10(8):3112–27.